Computerized Medical Imaging and Graphics 36 (2012) 610–619

Contents lists available at SciVerse ScienceDirect

Computerized Medical Imaging and Graphics

journal homepage: www.elsevier.com/locate/compmedimag

Anatomically guided voxel-based partial volume effect correction in brain PET: Impact of MRI segmentation

Daniel Gutierrez[a], Marie-Louise Montandon[a], Frédéric Assal[b], Mohamed Allaoua[a], Osman Ratib[a], Karl-Olof Lövblad[c], Habib Zaidi[a,d,e,*]

[a] Division of Nuclear Medicine and Molecular Imaging, Geneva University Hospital, CH-1211 Geneva, Switzerland
[b] Neurology Clinic, Geneva University Hospital, CH-1211 Geneva, Switzerland
[c] Division of Neuroradiology, Geneva University Hospital, CH-1211 Geneva, Switzerland
[d] Geneva Neuroscience Center, Geneva University, CH-1205 Geneva, Switzerland
[e] Department of Nuclear Medicine and Molecular Imaging, University of Groningen, University Medical Center Groningen, 9700 RB Groningen, Netherlands

ARTICLE INFO

Article history:
Received 11 May 2012
Received in revised form 7 August 2012
Accepted 7 September 2012

Keywords:
MRI
PET
Brain imaging
Segmentation
Partial volume effect

ABSTRACT

Partial volume effect is still considered one of the main limitations in brain PET imaging given the limited spatial resolution of current generation PET scanners. The accuracy of anatomically guided partial volume effect correction (PVC) algorithms in brain PET is largely dependent on the performance of MRI segmentation algorithms partitioning the brain into its main classes, namely gray matter (GM), white matter (WM), and cerebrospinal fluid (CSF). A comparative evaluation of four brain MRI segmentation algorithms bundled in the successive releases of Statistical Parametric Mapping (SPM) package (*SPM99*, *SPM2*, *SPM5*, *SPM8*) using clinical neurological examinations was performed. Subsequently, their impact on PVC in ^{18}F-FDG brain PET imaging was assessed. The principle of the different variants of the image segmentation algorithm is to spatially normalize the subject's MR images to a corresponding template. PET images were corrected for partial volume effect using GM volume segmented from coregistered MR images. The PVC approach aims to compensate for signal dilution in non-active tissues such as CSF, which becomes an important issue in the case of tissue atrophy to prevent a misinterpretation of decrease of metabolism owing to PVE. The study population consisted of 19 patients suffering from neurodegenerative dementia. Image segmentation performed using *SPM5* was used as reference. The comparison showed that previous releases of SPM (*SPM99* and *SPM2*) result in larger gray matter regions (~20%) and smaller white matter regions (between −17% and −6%), thus introducing non-negligible bias in PVC PET activity estimates (between 30% and 90%). In contrary, the more recent release (*SPM8*) results in similar results (<1%). It was concluded that the choice of the segmentation algorithm for MRI-guided PVC in PET plays a crucial role for the accurate estimation of PET activity concentration. The segmentation algorithm embedded within the latest release of SPM satisfies the requirement of robust and accurate segmentation for MRI-guided PVC in brain PET imaging.

Published by Elsevier Ltd.

1. Introduction

Molecular brain imaging using positron emission tomography (PET) has emerged as one of the most promising modalities that steadily gained importance in the clinical and research arenas [1]. Considerable progress has been made to optimize the design of dedicated high resolution PET scanners and to integrate multimodality images to correlate functional findings to anatomy through the use of CT and MRI and to improve the quality and quantitative accuracy of brain PET images, however, emerging clinical and research applications of functional brain imaging promise even greater levels of accuracy and precision and therefore impose more constraints with respect to the information provided to clinicians and research scientists [2]. Since MRI is more suitable than CT for brain imaging owing to its high soft tissue contrast and better spatial resolution, combined PET-MRI systems dedicated for brain imaging have emerged as alternatives to PET-CT [3]. One of the first steps to obtain the best of the various imaging modalities is to coregister functional and anatomical images, and to a pre-segmented atlas if available. Wu et al. [4] has shown that this task can be optimized using non-rigid registration procedures compared to rigid or semi-rigid procedures such as those implemented in the Automated Image

* Corresponding author at: Division of Nuclear Medicine and Molecular Imaging, Geneva University Hospital, CH-1211 Geneva, Switzerland. Tel.: +41 22 3727258; fax: +41 22 3727169.
E-mail address: habib.zaidi@hcuge.ch (H. Zaidi).

0895-6111/$ – see front matter. Published by Elsevier Ltd.
http://dx.doi.org/10.1016/j.compmedimag.2012.09.001

Registration (AIR) and the Statistical Parametric Mapping (SPM) packages. These techniques are, however, especially useful when dealing with inter-subject image registration.

Unfortunately PET imaging suffers from many physical degrading effects, partial volume effect (PVE), which is common to all medical imaging techniques owing to the discrete sampling of the image formation process, being one of them. In brain PET imaging, this effect is not negligible owing to the large voxel size, which produces images where high activity regions spillover into low activity regions, potentially leading to erroneous results in the qualification of functional brain imaging [5,6]. Since neurological PET imaging was developed very early, the first attempts to reduce the impact of the PVE and restore the image content focused on brain imaging [7]. This has been addressed through the calculation of recovery coefficients [8], thus limiting the methods to the use of only PET data, since in these early years multimodality imaging was still not readily available as it is nowadays. The advent of modern multimodality imaging, and particularly brain PET/MR, stimulated the development of new partial volume correction (PVC) techniques which exploit a priori information gathered from anatomical information through partitioning MR images into different compartments, typically gray matter (GM), white matter (WM), and cerebrospinal fluid (CSF) [9]. More recently, a novel class of PVC algorithms that do not require segmentation of anatomical images was introduced [10]. This includes very promising approaches such as the wavelet decomposition technique [11] and the Bayesian approach [12]. In both cases, the algorithm is able to find the high frequency information lacking in low resolution PET images at a voxel-level without increasing the noise.

Current PVC algorithms that require the segmentation of anatomical images correct functional PET images in the projection space, during the reconstruction process or after their reconstruction (post-reconstruction) at regional level using a region-of-interest (ROI)-based analysis or in a more general way at the voxel level (voxel-based) [13]. Among ROI-based post-reconstruction methods, the most popular techniques use recovery coefficients [7,8] or the geometric transfer matrix (GTM) method [14,15] used in our previous work [16]. The principle of ROI-based methods is to calculate the effective activity in different regions assuming that the tracer uptake in each particular region is homogeneous. Naturally, the complexity of the problem increases when the number of considered regions increases, rendering PVC of the whole brains a complex problem. Nevertheless, in a simple case using ROIs has shown promising results [15].

Conversely, voxel-based approaches are not limited to a particular ROI since they attempt to recover the actual activity concentration in the cortex on a voxel-by-voxel basis, though with a priori assumptions about the tracer distribution [10,17,18]. These techniques have the advantage of generating corrected image for qualitative assessment and visual interpretation. The principal drawback of voxel-based methods compared to ROI-based methods is that they are quantitatively less accurate and rely on many assumptions. Partition methods are one example of voxel-based methods, the simplest case being to define one unique partition corresponding to brain tissue classes (GM and WM) and to compensate the spillover on non-active regions (CSF) by converting PET intensities from activity per spatial volume to activity per tissue volume [19]. This is achieved by convolving the partition (brain mask) with the point spread function (PSF) of the PET imaging system. This approach was extended to two (GM and WM) [20] and three compartments assuming that the CSF activity is not only the result of spillover from contiguous regions [18].

MR image segmentation is the critical component of MRI-guided PVC in brain PET imaging [14,17,21]. In a previous work, we compared the impact of various MR image segmentation algorithms on the GTM algorithm for PVC of ^{18}F-FDG and ^{18}F-FDOPA brain PET data [16]. One of the conclusions of this work was that Statistical Parametric Mapping (*SPM2*) segmentation software is more suitable for clinical routine examinations owing to the robustness of its normalization algorithm for atypical brains.

In this work, we aim to assess the influence of 4 chronologically successive releases of SPM segmentation software on a voxel-based PVC method proposed by Matsuda et al. [9] in contrast to previous work referenced above.

2. Materials and methods

2.1. Brain MRI segmentation algorithms

SPM is among the well established packages used for statistical analysis of neuroimaging data including PET, SPECT and fMRI [22]. It is well-documented, freely available, technically supported by well established brain imaging centers [23] and widely used by the neuroimaging community. The brain MR image segmentation technique implemented in this package considers the three tissue classes of interest for PVC, namely gray matter (GM), white matter (WM), and cerebrospinal fluid (CSF).

A comparative evaluation of the impact of brain MRI segmentation algorithms on PVC in ^{18}F-FDG PET imaging was performed using the implementations embedded in the last four successive releases of SPM, namely *SPM99*, *SPM2*, *SPM5* and *SPM8*. The main steps of the SPM segmentation algorithm are:

- Spatial normalization involving the transformation of the subject's images to corresponding template image;
- Segmentation of the images into a limited number of clusters (k). In this case the clusters correspond to GM, WM, CSF and background [24];
- Preprocessing of the segmentations through convolution with an isotropic Gaussian kernel to obtain the cluster concentration representing the probability distribution that the voxel belongs to a given region (GM, WM, or CSF).

A detailed description of the history of SPM and evolution of the segmentation toolbox is beyond the scope of this paper. Nevertheless, we give a brief description of the evolution of the MRI segmentation toolbox implemented in the SPM package for the above mentioned versions. One must note that *SPM99* [25], the earliest version used in this work, is already the 5th release of the SPM package [22]. This version has consolidated the image normalization procedure by introducing penalization factors on the non-linear deformation to obtain more robust invertible deformations. The *SPM2* release marked a turning point on the SPM software since this version introduced the Bayesian framework to replace the frequentist methods. *SPM5* release has consolidated the Bayesian formulation introduced in the previous version by its generalization in all the modules of the software. In the image registration and normalization this was made replacing the mean squared difference minimization between the subjects with Bayesian prior probabilities [26] allowing spatial normalization of different MRI sequences without the need to construct sequence-specific templates. The statistical analysis was also modified to include Bayesian formulation using spatial smoothness priors.

SPM8 version is the most recent release dating back to April 2009. The unified segmentation was rendered more stable by modeling, not only the brain, but the entire head using the Diffeomorphic Anatomical Registration Through Exponentiated Lie-algebra (DARTEL) [27]. These are deformations parameterized by a single flow field intended to obtain more accurate image registration between the brains of different subjects. This new version included routines for the construction of posterior probability maps

to be used with the Bayesian formulation in the statistical inference part.

The 4 versions of SPM segmentation were used to segment clinical T1-weighted MR brain images and the resulting partitions fed as input into the 2 compartment voxel-based PVC algorithm described in the following section. In the absence of ground truth for comparative assessment of clinical studies, we have chosen *SPM5* segmentation and the resulting PVC PET images as reference. This choice is justified by the fact that at the time the study started, this was the most stable version of the SPM software.

2.2. Partial volume effect correction

Partial volume correction was performed using the method proposed by Matsuda et al. [9]. The algorithm uses utilities available in *SPM99* for image registration and MRI segmentation by default. The algorithm comprises the following 10 steps:

1. The scalp of MR images is removed by binary masking of the whole brain;
2. Original MR and PET images are registered using rigid-body transformation (6 degrees of freedom: 3 translations and 3 rotations). This step was performed on the Hermes platform (Hermes MultiModality™, Nuclear Diagnostics AB, Sweden);
3. The segmented white and gray matter images are convolved with the PSF of the PET scanner to obtain dispersion coefficients. Since the radial spatial resolution varies from 4.1 @ 1 cm to 4.9 mm @ 10 cm offset while the axial spatial resolution varies from 4.6 to 5.5 cm, we took an average full width at half maximum of 5 mm of the 3D Gaussian PSF for our system;
4. The convolved images are normalized to have a maximum floating point value (32 bits) of 1;
5. A binary image is created from the normalized convolved GM image using a threshold of 0.2 (20% of maximum). This image will serve as a mask for the GM;
6. A whole brain image mask is created from the mask of the GM (of step 5) by filling interior holes;
7. A WM PET image is simulated from the normalized WM image (of step 4) by replacing its maximum (1.0) value with the maximum PET counts in WM. This maximum PET count is calculated through an automatic ROI determined by setting a threshold above 95% of the maximum count density of the white matter MR images (of step 4);
8. The GM PET images are obtained by subtracting the WM PET images (of step 7) from the original PET images (of step 2);
9. Finally, the GM PET image is divided by the normalized GM MR image (of step 4), and masked with the GM binary mask (of step 5);
10. One constraint on the procedure is fixed to avoid edge effects by limiting the maximum corrected voxel value to be lower or equal to the maximum uncorrected voxel value.

2.3. Clinical data acquisition

Nineteen patients suspected to suffer from neurodegenerative dementia were referred to the Nuclear Medicine Division of Geneva University Hospital for a PET/CT scan using [^{18}F]-fluorodeoxyglucose (FDG). Their age ranged from 50 to 91 years (mean ± SD = 72 ± 9.15). PET/CT data acquisition was performed on a Biograph HiRez Sensation 16 (Siemens Healthcare, Erlangen, Germany) using a standard protocol recommended by the manufacturer. PET acquisition was started approximately 30 min after injection of 370 MBq of [^{18}F]-FDG. The PET emission study (20 min, 1 bed position) followed immediately the CT study (120 kVp, 320 mA s, 16 × 0.75 collimation, a pitch of 0.8 and 1.5 s per rotation) used for attenuation correction. The 3D PET sinograms were corrected for detector sensitivity, dead time, random coincidences, scatter and attenuation, and converted to 2D sinograms using Fourier rebinning. A filtered backprojection algorithm was used for PET image reconstruction.

MR images were acquired on a Philips 1.5-T Eclipse scanner (Philips Medical Systems, Best, The Netherlands) using a 3D T1-weighted gradient-echo sequence. The parameters were as follows: TR = 15 ms, TE = 4.4 ms and a flip angle of 25°. Image matrix consisted of 256 × 256 × 160 voxels, with a resolution in the transaxial direction of 0.97 mm × 0.97 mm, and an axial resolution of 1.1 mm.

2.4. Comparative assessment strategy

The quantitative assessment of the performance of different segmentation algorithms was performed by comparing the segmentation results of the different versions of SPM with the *SPM5* segmented images for each tissue class relevant for PVC (GM and WM). Moreover, the impact of MR image segmentation on PVC estimates in ^{18}F-FDG brain PET studies was evaluated by calculating the linear regression for each paired combination of corrections realized using 2 different segmentation algorithms. Quantification of the agreement between the corrections realized using 2 segmentation algorithms was also performed using Bland and Altman statistical analysis by plotting the difference against the average of the compared methods [28]. The relative difference between the corrections using 2 different segmentation algorithms was defined as:

$$\text{Percent difference} = \frac{VOI_{method} - VOI_{SPM5}}{VOI_{SPM5}} \times 100\%$$

where VOI_{method} is the activity concentration in a particular volume of interest (VOI) calculated on the PVE corrected PET image segmented using the considered method, whereas VOI_{SPM5} is the activity concentration in the same VOI calculated on the PVE corrected PET image segmented using *SPM5*. We assessed 20 symmetric VOIs for each patient that are listed below with their abbreviations:

	Left	Right
Gyrus frontalis superior	LGFS	RGFS
Gyrus frontalis inferior	LGFI	RGFI
Gyrus temporalis medius	LGTM	LGTM
Gyrus supramarginalis	LGS	RGS
Cuneus	LC	RC
Precuneus	LPREC	RPREC
Hippocampus	LH	RH
Thalamus	LT	RT
Putamen	LP	RP
Caput nuclei caudati	LCNC	RCNC

To further assess the PVC method in an absolute manner, we calculated the mean recovery coefficients for each of the 20 previously defined VOIs as the ratio of the uncorrected to PVC corrected activity concentration values.

3. Results

3.1. Comparison of brain MRI segmentation methods

Figs. 1 and 2 show representative slices of a clinical T1-weighted MR study and the corresponding segmentation results when using the 4 segmentation algorithms. Images of GM and WM regions are shown separately. The first observation one can formulate is that non-brain matter is often included into the GM region of segmentations performed using *SPM99*.

Table 1 shows the relative differences between the 4 segmentation algorithms with respect to GM and WM volume calculation

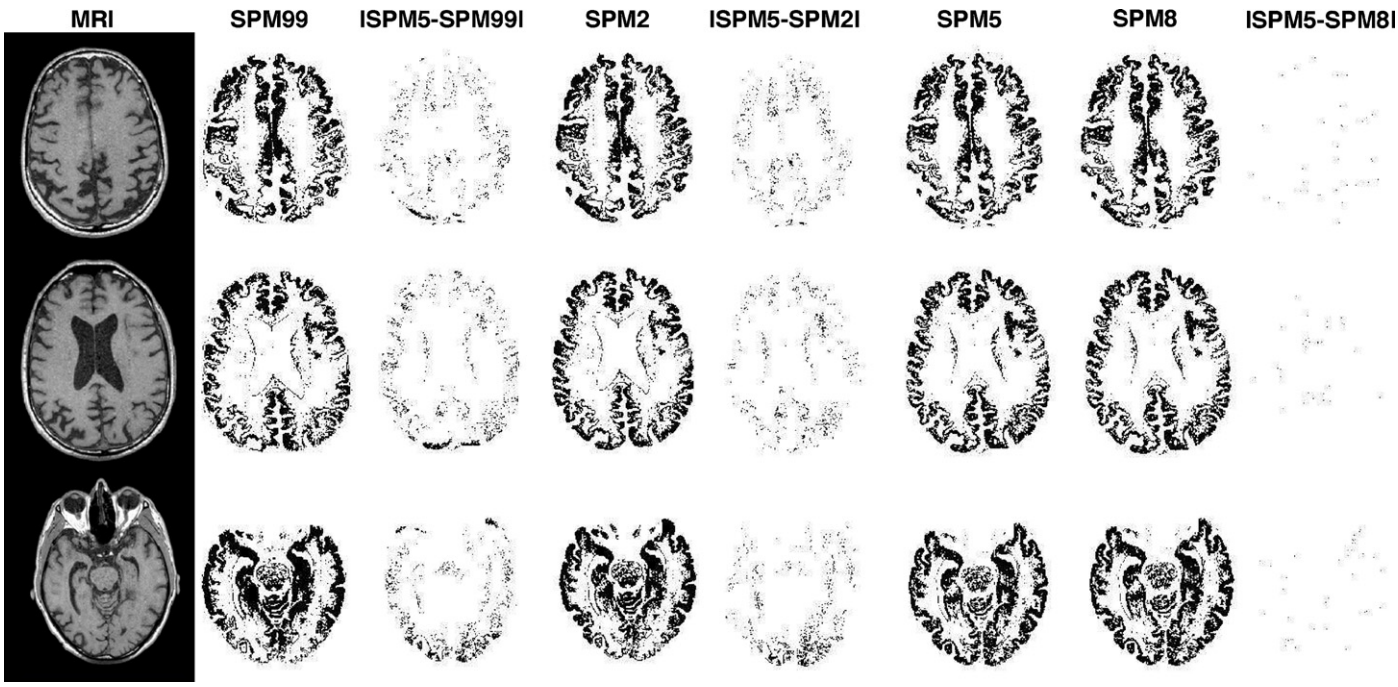

Fig. 1. Transverse views of gray matter segmentation of a MR image of a patient with probable Alzheimer's disease. From left to right: Original MRI, *SPM99*, $|SPM5 - SPM99|$, *SPM2*, $|SPM5 - SPM2|$, *SPM5, SPM8*, $|SPM5 - SPM8|$.

of clinical brain MR images. Overall, there is a large variability in the difference between the volumes ranging from 0.001 to 62%. For the GM, a low correlation was observed between the segmentation algorithms of the first 3 versions of SPM. However, a high correlation was obtained between *SPM5* and *SPM8* as expected. Similar observations were made for WM.

3.2. Impact on partial volume effect correction

Fig. 3 shows a representative example illustrating the impact of MRI segmentation on partial volume correction of FDG brain PET images in a patient with probable Alzheimer's disease. Partial volume effect correction improves the resolution of brain PET images. One can see that differences between PVC PET images when comparing various segmentation techniques to *SPM5* algorithm appear mainly on the boundaries of the brain when using *SPM99* and *SPM2* while *SPM8* produces similar results compared to *SPM5*.

The mean relative differences for the 19 clinical studies summarized in Table 2 substantiate the qualitative results. One can see that the mismatch between segmentations performed using *SMP99* and *SPM2* compared to the one obtained with *SPM5* introduce an

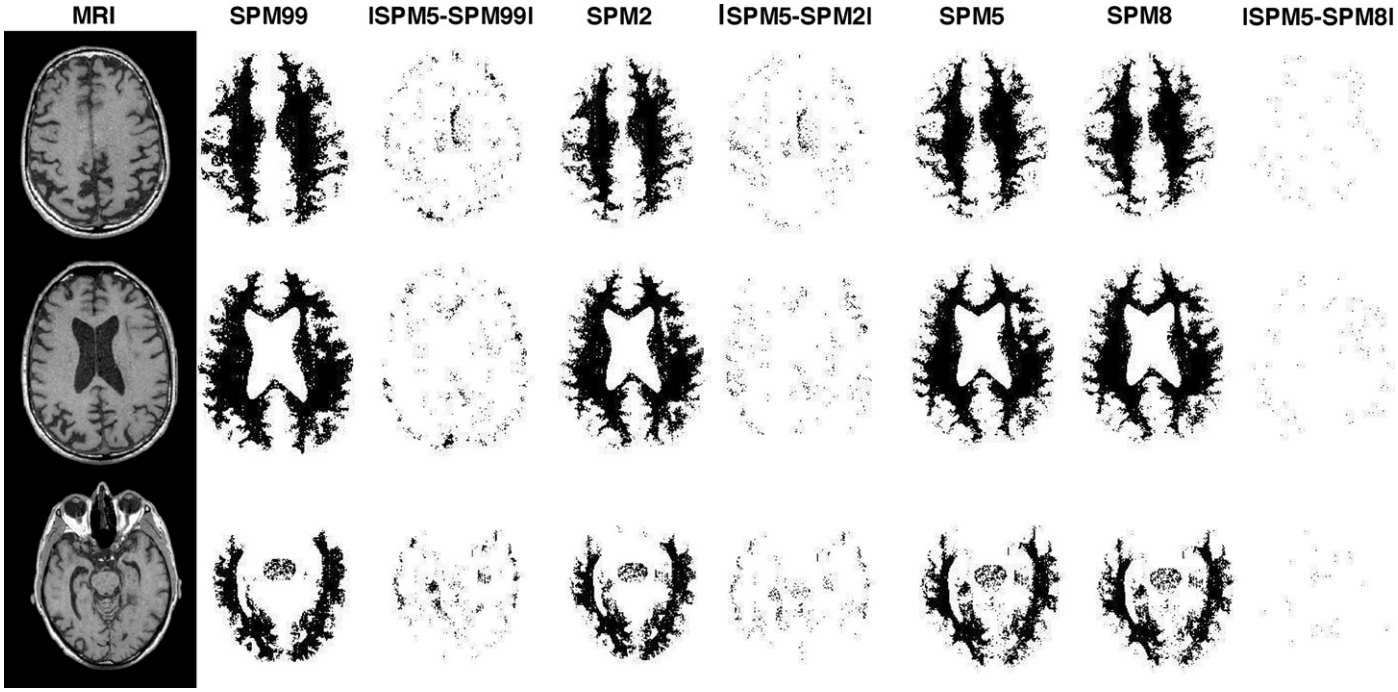

Fig. 2. Same as Fig. 1 for white matter segmentation.

Table 1
Relative differences (%) between the 4 segmentation algorithms with respect to gray matter (GM) and white matter (WM) volume estimates of the clinical MR images after realignment to PET images. The differences are calculated on the basis of the segmentation implemented in *SPM5*.

	GM			WM		
	$(SPMx - SPM5)/SPM5 \times 100\%$			$(SPMx - SPM5)/SPM5 \times 100\%$		
SPMx	*SPM99*	*SPM2*	*SPM8*	*SPM99*	*SPM2*	*SPM8*
Patient 1	31.91	24.79	0.00	−12.05	−5.92	0.00
Patient 2	62.28	54.40	1.16	−17.13	−8.10	−0.49
Patient 3	16.36	27.28	−1.19	−19.90	−6.35	0.01
Patient 4	16.84	20.08	−0.01	−19.08	−13.57	−0.06
Patient 5	16.19	21.17	0.00	−19.89	1.46	0.00
Patient 6	13.92	9.49	0.17	−11.25	−4.16	−0.02
Patient 7	13.95	18.74	−0.84	−13.47	7.33	−0.62
Patient 8	18.93	20.94	0.02	−20.43	−8.44	0.00
Patient 9	13.98	16.34	0.01	−17.38	−12.63	0.00
Patient 10	25.62	18.40	−0.03	−16.27	−6.74	−0.03
Patient 11	44.51	20.00	0.01	−28.49	−4.40	0.02
Patient 12	12.50	12.23	0.73	−8.26	−4.97	−0.71
Patient 13	25.38	21.40	−0.01	−16.28	−3.79	−0.01
Patient 14	28.83	23.47	0.00	−28.46	−12.14	0.00
Patient 15	8.11	5.93	−0.01	−19.65	−5.08	0.03
Patient 16	10.15	6.78	0.16	−21.67	−6.57	1.03
Patient 17	18.18	15.15	0.10	−15.32	−3.61	−0.02
Patient 18	14.25	12.91	0.15	−14.58	−11.43	0.03
Patient 19	19.40	19.76	−0.08	−17.92	−6.53	0.03
Mean	21.65	19.44	0.02	−17.76	−6.09	−0.04
SD	13.12	10.29	0.48	5.12	4.90	0.35

overcorrection in the PVC recovered activity. This is particularly noticeable for the white matter resulting in mean relative differences of 91.8% and 71.3% for *SMP99* and *SPM2*, respectively. This overcorrection is lower for the gray matter but still remains high (37.3% and 29.8% for *SMP99* and *SPM2*, respectively). Likewise, there is good agreement between *SPM8* and *SPM5* with relative difference of 0.3% and 0.76% for gray and white matter, respectively.

The mean recovery coefficients calculated for the 20 defined VOIs are summarized in Table 3. One can see that the general trend is that the recovery coefficients slightly increase when using *SPM99* compared to *SPM2* and *SPM5* segmentations. The latter produces almost similar results compared to *SPM8*.

Figs. 4 and 5 show linear correlation plots between the recovered activity estimates obtained using the 3 segmentation algorithms versus *SPM5* for gray and white matter, respectively. It can be seen that the slope of the regression line for the GM is very close to 1 for all segmentation algorithms; however, the correlation coefficient (R^2) is below 0.8 for *SPM99* and *SPM2* showing that the relationship between the results is in some way random. On the other hand, the correlation coefficient is almost 1 for *SPM8* showing that the segmentation achieved with *SPM8* is equivalent to those obtained with *SPM5*. The situation is worst for the WM as shown on Table 2 since the correlation coefficients for *SPM99* and *SPM2* are below 0.2 with slopes around 0.5. This indicates that there is almost no

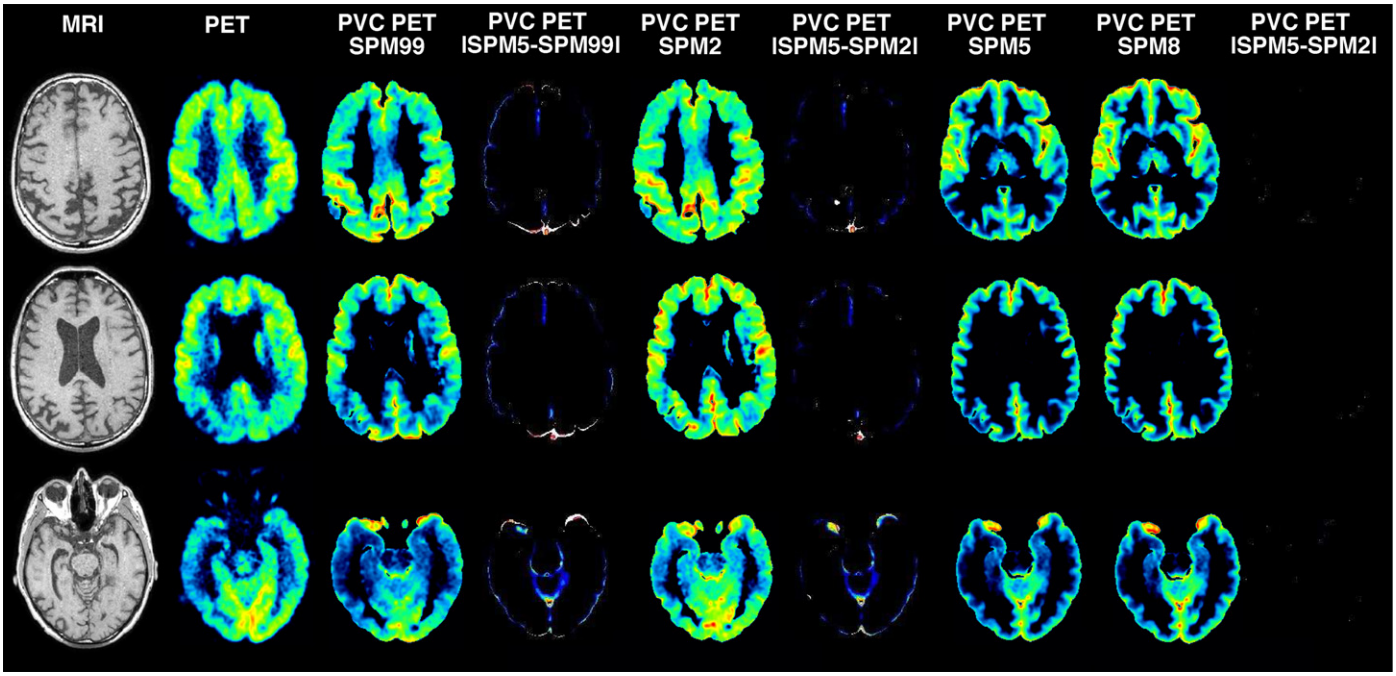

Fig. 3. Illustration of the impact of the segmentation method on the partial volume correction in functional brain PET imaging for a patient with probable Alzheimer's disease, presented in the same order as Figs. 1 and 2.

Table 2
Relative difference (%) between activity concentration estimates in gray matter (GM) and white matter (WM) after PVC when using the four segmentation algorithms on clinical ^{18}F-FDG brain PET images. The differences are calculated with respect to *SPM5* segmentation algorithm.

	GM			WM		
	$(SPMx - SPM5)/SPM5 \times 100\%$			$(SPMx - SPM5)/SPM5 \times 100\%$		
SPMx	*SPM99*	*SPM2*	*SPM8*	*SPM99*	*SPM2*	*SPM8*
Patient 1	33.18	24.65	1.71	67.90	−1.69	1.76
Patient 2	69.45	68.06	1.82	104.80	98.31	2.22
Patient 3	31.73	38.01	−0.20	48.81	54.04	−0.55
Patient 4	35.94	35.41	0.05	98.85	28.83	−0.15
Patient 5	37.32	28.73	0.00	110.48	68.54	0.00
Patient 6	13.20	12.98	0.23	7.63	30.89	0.39
Patient 7	31.86	26.84	1.22	180.35	228.92	8.91
Patient 8	33.08	33.62	0.01	58.84	33.20	−0.03
Patient 9	20.78	24.52	0.00	16.80	10.30	0.01
Patient 10	49.61	31.87	−0.16	119.47	68.63	−0.31
Patient 11	58.49	12.96	0.01	125.25	20.62	−0.02
Patient 12	52.83	56.02	1.73	218.98	264.20	0.87
Patient 13	33.74	23.07	0.00	66.91	16.87	0.00
Patient 14	45.90	36.07	−0.01	74.45	70.59	0.01
Patient 15	12.42	8.25	−0.02	5.52	21.00	0.04
Patient 16	36.41	26.12	−0.80	118.52	148.46	1.12
Patient 17	49.52	34.64	0.10	205.92	149.28	0.02
Patient 18	27.65	21.20	0.13	63.21	17.61	0.07
Patient 19	34.79	23.90	−0.06	51.63	25.85	0.06
Mean	37.26	29.84	0.30	91.79	71.29	0.76
SD	14.49	14.14	0.74	61.12	75.31	2.10

correlation between these results. *SPM8* algorithm is closely related and well correlated with *SPM5* ($R^2 = 0.998$, slope very close to 1). These results are further confirmed by Bland and Altman plots for gray and white matter (Figs. 6 and 7).

Linear regression analysis was also performed between recovered activity estimates obtained using *SPM5* and those obtained using the 3 other segmentation algorithms for the 20 VOIs. The resulting slopes and correlation coefficients for the 19 patients are reported in Fig. 8. It can be seen that, except few cases, *SPM99* (for patients 6, 7, and 18) and *SPM2* (for patients 6, 8 11 and 18) segmentations are uncorrelated with *SPM5* segmentation, whereas excellent correlation could be observed between *SPM8* and *SPM5* segmentations except a single study (patient 19).

Figs. 9 and 10 show the relative differences between regional cerebral glucose metabolism (rCGM) estimated using the various algorithms compared to *SPM5* segmentation. Similar observations

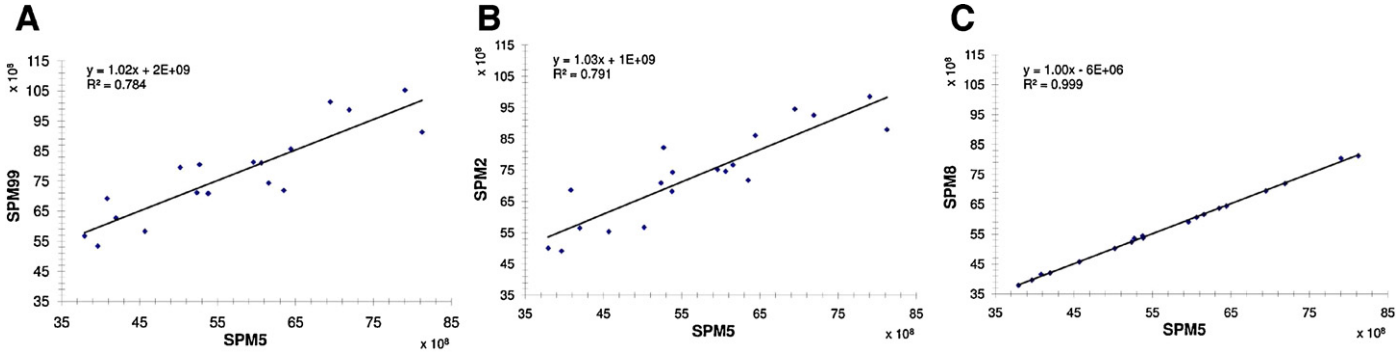

Fig. 4. Correlation plots between partial volume corrected activity values of 3D brain scans comparing results obtained using *SPM5* (abscissa) and (A) *SPM99*, (B) *SPM2*, and (C) *SPM8* (ordinate) together with best fit equations and correlation coefficients for gray matter.

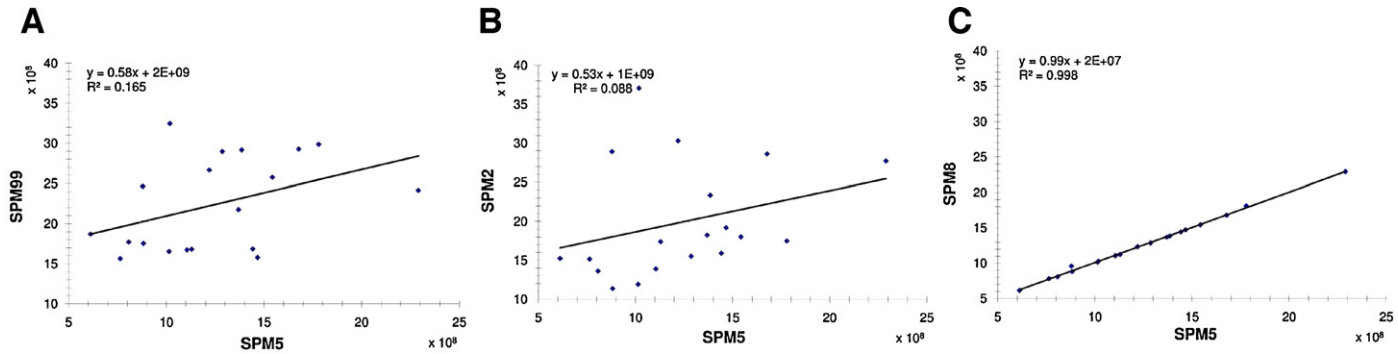

Fig. 5. Same as Fig. 4 for white matter.

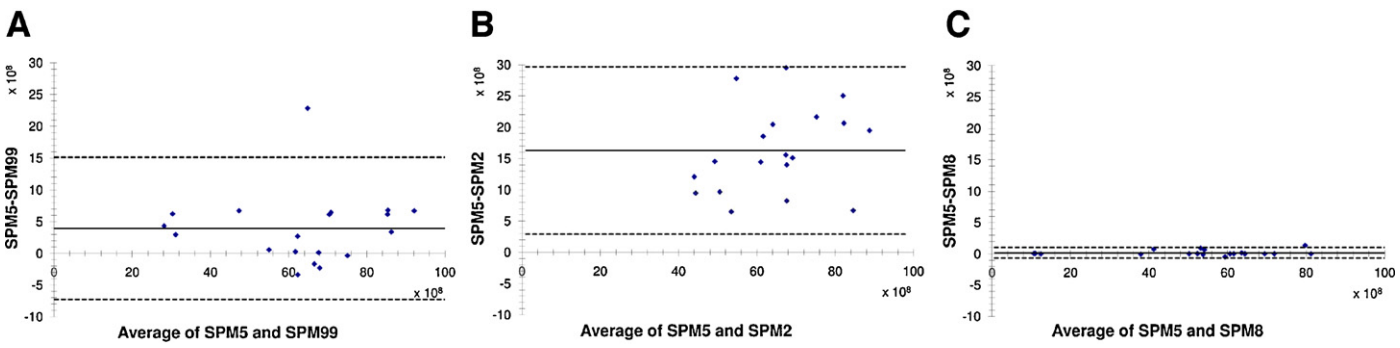

Fig. 6. Bland and Altman plots showing difference partial volume corrected activity values obtained using (A) *SPM99*, (B) *SPM2* and (C) *SPM8* methods against *SPM5* method for the gray matter. The middle line is the mean, and the upper and lower broken lines are the mean ± 1.96 * SD.

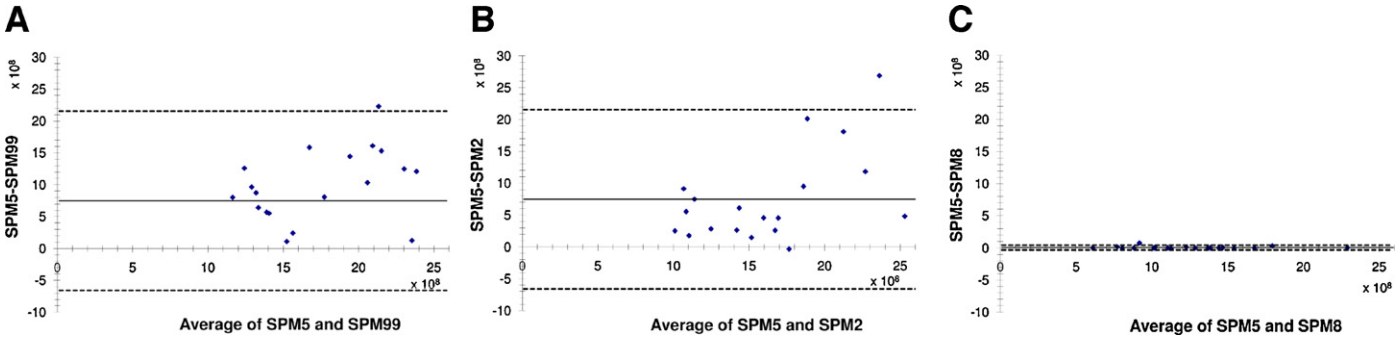

Fig. 7. Same as Fig. 6 for white matter.

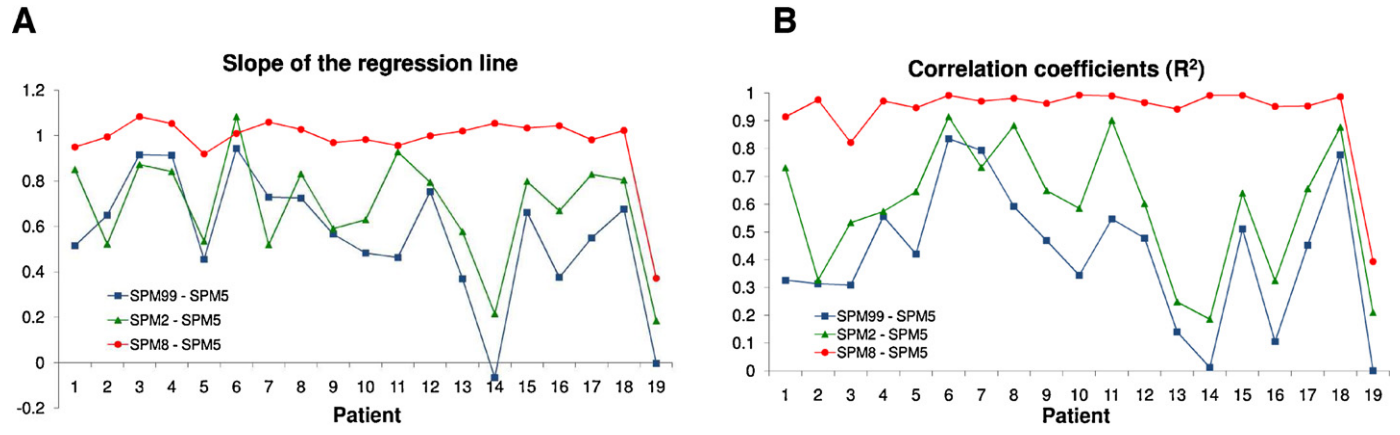

Fig. 8. Plots of slopes and correlation coefficients (R^2) for each patient resulting from linear regression analysis between PET PVEC 99 and PET PVEC 5, between PET PVEC 2 and PET PVEC 5, and PET PVEC 8 and PET PVEC 5 for 20 VOIs: (A) the slopes of the regression lines; (B) the correlation coefficients.

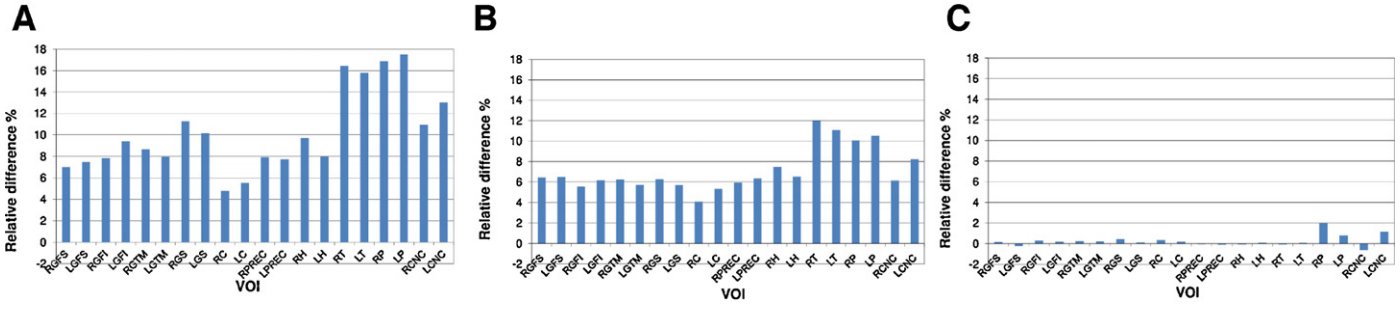

Fig. 9. Relative differences between absolute rCGM estimates for PET PVEC 5 and (A) PET PVEC 99, (B) PET PVEC 2, (C) PET PVEC 8 for the 20 VOIs studied.

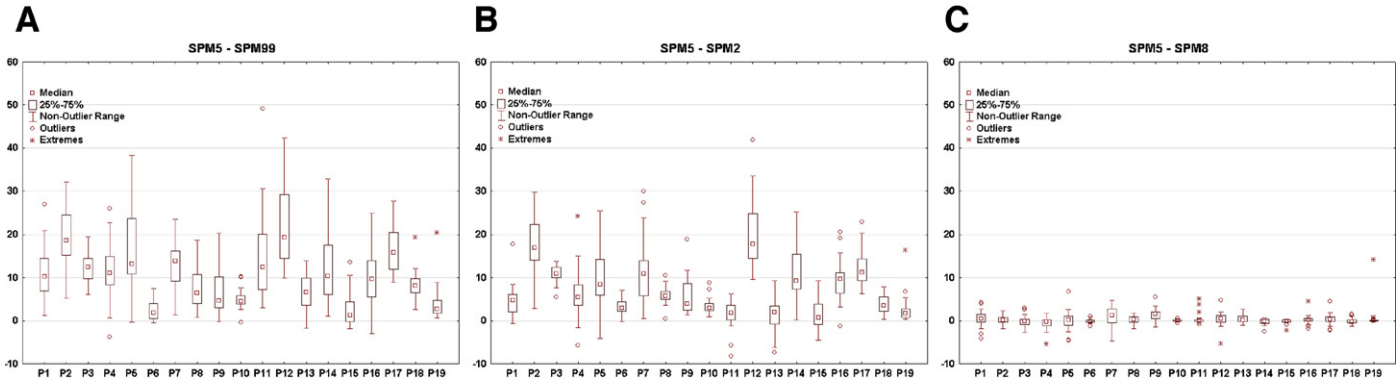

Fig. 10. Box and Whisker plots showing relative differences between absolute rCGM with respect to PET PVEC 5 of (A) PET PVEC 99, (B) PET PVEC 2, and (C) PET PVEC 8. The median, 10, 25, 75 and 90 percentiles are calculated over the 20 VOIs for each of the 19 patients studied.

can be made in the sense that, depending on the VOI, *SPM99* and *SPM2* result in large relative differences compared to *SPM5* while *SPM8* produce relatively small differences. One can also notice that right and left putamen (RP and LP) as well as right and left caput nuclei caudati (RCNC and LCNC) present with the highest differences in all comparisons. The right and left thalamus (RT and LT) present with the largest differences when using *SPM99* and *SPM2*. The relative errors averaged over all regions for each patient are below 5% for some clinical studies (patients 5, 10, 15 and 19) when comparing *SPM99* and *SPM5* but at least 11 cases present with relative differences of at least 10%. The relative differences between *SPM2* and *SPM5* are slightly lower since most of the cases present with values lower that 10%. Similarly, *SPM8* presents with the lowest relative errors (<3%).

4. Discussion

It is well established that PVC improves image quality and quantitative accuracy of functional PET imaging where the image degradation resulting from the PVE is higher as a consequence of their poor image resolution. PVC is crucial to avoid misinterpretation of functional brain PET data [5]. Unfortunately, the performance of PVC algorithms is highly dependent on accuracy of the various steps involved in the procedure in a complex way.

Table 3
Mean recovery coefficients (%) over the 19 patients calculated for 20 VOIs.

	SPM99	*SPM2*	*SPM5*	*SPM8*
RGFS	56.0	56.3	59.9	59.8
LGFS	56.3	56.8	60.5	60.6
RGFI	56.8	58.0	61.2	61.0
LGFI	55.6	57.3	60.8	60.7
RGTM	52.1	53.3	56.7	56.5
LGTM	52.1	53.2	56.2	56.1
RGS	51.8	54.2	57.6	57.4
LGS	51.8	54.0	57.0	57.0
RC	63.2	63.6	66.2	66.0
LC	62.5	62.6	65.9	65.8
RPREC	59.2	60.3	63.9	63.9
LPREC	58.8	59.6	63.3	63.4
RH	50.9	51.9	55.8	55.8
LH	51.5	52.2	55.7	55.6
RT	56.1	58.3	65.3	65.3
LT	56.8	59.2	65.7	65.7
RP	63.0	66.9	73.6	72.2
LP	63.0	67.0	74.0	73.4
RCNC	57.8	60.4	64.1	64.5
LCNC	55.2	57.6	62.4	61.7
Mean	56.5	58.1	62.3	62.1
SD	4.1	4.5	5.3	5.1

Overall, with one exception [29], it has been reported that the accuracy of MRI segmentation has a higher impact on the accuracy of the PVC activity concentration estimates compared to the influence of image co-registration [18,21,30].

This study focused on the impact of four MRI brain segmentation algorithms embedded in various version of the SPM software on MRI-guided voxel-based PVC using clinical FDG-PET data. The first observation regarding the segmentation algorithm is that newer versions of SPM (starting from *SPM5*) seem to produce more reliable segmentation of brain images. We have demonstrated in this work that previous versions of SPM produce mis-segmentation errors, thus overestimating the size of GM while underestimating the size of WM.

This is probably due to the implementation of new and more sophisticated computational approaches, mainly the utilization of the Bayesian framework that was not used in *SPM99*. Note that this version results in the largest differences compared to *SPM5*. Even if *SPM2* incorporates this kind of analysis, it appears that the early implementation was not efficient enough and was consolidated only in *SPM5* [22].

The differences between MRI segmentation algorithms highly influence partial volume correction of PET data; however, the relationship between the results of MRI segmentation algorithms and PVC of brain PET data is not trivial since PVE correction is not a linear process. Nevertheless, it should be noted that they seem to be in some way linked because higher differences between MRI segmentations (Table 1) produce higher differences in recovered activity estimates (Table 2), and higher recovery coefficients (Table 3).

Several studies assessed the influence of PET-MR image registration and MR image segmentation errors on the accuracy of PVC algorithms [14,18]. This has been investigated for both the region-based [14,15,29,31] and voxel-based approaches [18,29,30,32]. It has been reported that the influence of the accuracy of the image registration procedure on the GTM approach is small (less than 2%) compared to the accuracy of the MRI segmentation procedure (∼5%). However, this error affects only the mis-segmented regions [14]. Likewise, Muller-Gartner et al. [18] have shown that their voxel-based 3-compartment partition method is less sensitive to mis-registration errors (−6% to 2.5% for a shift of −3 to 3 pixels) than to mis-segmentation errors (−20% to 30% for a mismatch of −3 to 3 pixels).

The implementation of the voxel-based PVC method used in this work [9] bears some similarities to Muller-Gartner's method [18] and as such has similar properties and presents with a similar behavior. In our case, an overestimation of GM volume (mean of about 22%) produces an overestimation of the GM recovered activity concentration by about 37% in the worst case (*SPM99*). This higher value is in agreement with observations made by

Muller-Gartner et al. [18] which have reported an error in the order of 5% in GM PET estimate for a 20% error in WM tracer concentration. It should be noted that the later is a 3-compartment method in contrast to the 2-compartment method (GM and WM) adopted by Matsuda et al. [9].

Bland and Altman analysis (Figs. 6 and 7) further confirmed that PET PVC activity estimates obtained using *SPM99* and *SPM2* are poorly related to results obtained using *SPM5*. *SPM8* and *SPM5* are highly correlated since the mean values (x-axis) of these plots have a large spread while the difference between them is kept very low (y-axis).

It would be interesting to explore the impact of differences in brain MRI segmentation techniques on other voxel-based PVC approaches, such as the wavelet decomposition method [10]. On the other hand, alternative PVC approaches that do not require MRI segmentation, thus enabling to overcome the inaccuracies associated with this procedure were recently introduced. Given the limitations of deconvolution algorithms, their use will result in some degradation of the precision of the processed data and as such, a high variance associated with the corrected estimates [21]. Promising PVC strategies that are capable of compensating for resolution loss in PET images using the information present in the corresponding anatomical images are becoming available. One such promising approach is the mutual multiresolution analysis method using 3D wavelet decomposition of both anatomical and functional images combined with local analysis (using empirical parameters) to adapt the model according to regional information [11]. Another approach uses a Bayesian model that introduces the lacking information in the form of a priori probability of the high frequency activity presence considering as hypothesis the fact that the image formation is a linear combination of the actual activity concentration and a Gaussian noise [12]. The latter assumption could be at the origin of some artefacts seen on the image, though the obtained results are encouraging.

5. Conclusion

SPM is a popular software for multi-modal brain image analysis including a powerful toolbox for the challenging task of brain MR image segmentation. The introduction of novel segmentation methods and their implementation in new releases of this package have rendered older versions obsolete [22]. The Bayesian formulation introduced in *SPM2* and further consolidated in *SPM5* version was, probably, the most relevant improvement into SPM segmentation procedure. The segmentation algorithm embedded within the latest release of SPM satisfies the requirement of robust and accurate segmentation for MRI-guided PVC in brain PET imaging. It has been shown that the various versions of SPM produce substantially different MR segmentation results which impacts the PET recovered activity estimates. Therefore, conclusions drawn from using early versions of SPM segmentation toolbox should be verified.

Conflict of interest statement

The authors declare that they have no conflict of interest.

Acknowledgments

HZ and KL are supported by the Swiss National Science Foundation under grants SNSF 31003A-135576, 33CM30-124114 and 33CM30-140337. FA is supported by Fonds Cognitive Memory, NAC 08-025 and the Swiss National Science Foundation under grants 320030_138163/1 and SPUM 33CM30-124115.

References

[1] Sossi V. Cutting-edge brain imaging with positron emission tomography. PET Clin 2007;2:91–104.
[2] Zaidi H, Montandon M-L. The new challenges of brain PET imaging technology. Curr Med Imaging Rev 2006;2:3–13.
[3] Heiss W-D. The potential of PET/MR for brain imaging. Eur J Nucl Med Mol Imaging 2009;36:105–12.
[4] Wu M, Carmichael O, Lopez-Garcia P, Carter CS, Aizenstein HJ. Quantitative comparison of AIR, SPM, and the fully deformable model for atlas-based segmentation of functional and structural MR images. Hum Brain Mapp 2006;27:747–54.
[5] Meltzer CC, Cantwell MN, Greer PJ, Ben-Eliezer D, Smith G, Frank G, et al. Does cerebral blood flow decline in healthy aging? A PET study with partial-volume correction. J Nucl Med 2000;41:1842–8.
[6] Zaidi H, Sossi V. Correction for image degrading factors is essential for accurate quantification of brain function using PET. Med Phys 2004;31:423–6.
[7] Hoffman EJ, Huang SC, Phelps ME. Quantitation in positron emission computed tomography. 1. Effect of object size. J Comput Assist Tomogr 1979;3:299–308.
[8] Kessler RM, Ellis JR, Eden M. Analysis of emission tomographic scan data: limitations imposed by resolution and background. J Comput Assist Tomogr 1984;8:514–22.
[9] Matsuda H, Ohnishi T, Asada T, Li ZJ, Kanetaka H, Imabayashi E, et al. Correction for partial-volume effects on brain perfusion SPECT in healthy men. J Nucl Med 2003;44:1243–52.
[10] Shidahara M, Tsoumpas C, Hammers A, Boussion N, Visvikis D, Suhara T, et al. Functional and structural synergy for resolution recovery and partial volume correction in brain PET. Neuroimage 2009;44:340–8.
[11] Le Pogam A, Hatt M, Descourt P, Boussion N, Tsoumpas C, Turkheimer FE, et al. Evaluation of a 3D local multiresolution algorithm for the correction of partial volume effects in positron emission tomography. Med Phys 2011;38:4920–3.
[12] Wang H, Fei B. An MR image-guided, voxel-based partial volume correction method for PET images. Med Phys 2012;39:179–95.
[13] Rousset O, Rahmim A, Alavi A, Zaidi H. Partial volume correction strategies in PET. PET Clin 2007;2:235–49.
[14] Frouin V, Comtat C, Reilhac A, Gregoire MC. Correction of partial-volume effect for PET striatal imaging: fast implementation and study of robustness. J Nucl Med 2002;43:1715–26.
[15] Rousset OG, Ma Y, Evans AC. Correction for partial volume effects in PET: principle and validation. J Nucl Med 1998;39:904–11.
[16] Zaidi H, Ruest T, Schoenahl F, Montandon M-L. Comparative evaluation of statistical brain MR image segmentation algorithms and their impact on partial volume effect correction in PET. Neuroimage 2006;32:1591–607.
[17] Meltzer CC, Kinahan PE, Greer PJ, Nichols TE, Comtat C, Cantwell MN, et al. Comparative evaluation of MR-based partial-volume correction schemes for PET. J Nucl Med 1999;40:2053–65.
[18] Muller-Gartner HW, Links JM, Prince JL, Bryan RN, McVeigh E, Leal JP, et al. Measurement of radiotracer concentration in brain gray matter using positron emission tomography: MRI-based correction for partial volume effects. J Cereb Blood Flow Metab 1992;12:571–83.
[19] Videen TO, Perlmutter JS, Mintun MA, Raichle ME. Regional correction of positron emission tomography data for the effects of cerebral atrophy. J Cereb Blood Flow Metab 1988;8:662–70.
[20] Bataille F, Comtat C, Jan S, Sureau FC, Trebossen R. Brain PET partial-volume compensation using blurred anatomical labels. IEEE Trans Nucl Sci 2007;54:1606–15.
[21] Rousset O, Zaidi H. Correction of partial volume effects in emission tomography. In: Zaidi H, editor. Quantitative analysis of nuclear medicine images. New York: Springer; 2006. p. 236–71.
[22] Ashburner J. SPM: a history. Neuroimage 2012;62:791–800.
[23] Friston K, Ashburner J, Heather J, Holmes A, Poline JB. Statistical parametric mapping. London: The Wellcome Department of Cognitive Neurology, University College London; 1999.
[24] Ashburner J, Friston K. Multimodal image coregistration and partitioning – a unified framework. Neuroimage 1997;6:209–17.
[25] Ashburner J, Friston KJ. Voxel-based morphometry – the methods. Neuroimage 2000;11:805–21.
[26] Ashburner J, Friston KJ. Unified segmentation. Neuroimage 2005;26:839–51.
[27] Ashburner J. A fast diffeomorphic image registration algorithm. Neuroimage 2007;38:95–113.
[28] Bland JM, Altman DG. Statistical methods for assessing agreement between two methods of clinical measurement. Lancet 1986;1:307–10.
[29] Quarantelli M, Berkouk K, Prinster A, Landeau B, Svarer C, Balkay L, et al. Integrated software for the analysis of brain PET/SPECT studies with partial-volume-effect correction. J Nucl Med 2004;45:192–201.
[30] Strul D, Bendriem B. Robustness of anatomically guided pixel-by-pixel algorithms for partial volume effect correction in positron emission tomography. J Cereb Blood Flow Metab 1999;19:547–59.
[31] Slifstein M, Mawlawi O, Laruelle M. Partial volume effect correction: methodological consideration. In: Gjedde A, Hansen S, Knudsen GM, Paulson OB, editors. Physiological imaging of the brain with PET. San Diego (CA): Academic Press; 2001. p. 67–75.
[32] Meltzer CC, Zubieta JK, Links JM, Brakeman P, Stumpf MJ, Frost JJ. MR-based correction of brain PET measurements for heterogeneous gray matter radioactivity distribution. J Comput Assist Tomogr 1996;16:650–8.

Daniel Gutierrez received his Master in Physics in 2000 and his Minor in Infographics in 2003 from the University of Geneva to finally obtain his PhD in Life Sciences (Medical Imaging) in 2008 from the University of Lausanne, Switzerland. He is currently a Postdoc research fellow at the PET Instrumentation & Neuroimaging Laboratory (*PINLab*) at Geneva University Hospital (Switzerland). His research interests include medical image processing, dose optimization and multimodality imaging techniques.

Marie-Louise Montandon received the MS degree in Psychology and a PhD in Neuroscience from the universities of Geneva and Lausanne within the lemanic doctoral program in Neurosciences. She is an active member of the PET Instrumentation and Neuroimaging Laboratory (*PINLab*) of Geneva University. She is actively involved in developing imaging solutions for neuroscience research and clinical diagnosis. Her research centres on the development of improved methods for quantification of functional three-dimensional brain PET images using statistical image analysis tools. She is recipient of many awards and distinctions among which the 2005 best PhD thesis award given by the Medical School of Geneva University and the Research Grant for the Advancement of Women 2004 given by the Advisory Board for the Advancement of Women, National Center of Competence in Research CO-ME (Computer Aided and Image Guided Medical Interventions).

Frédéric Assal received his MD in 1988 then a medical doctorate thesis in plasticity of the visual system. He completed his medical training in neurology and a fellowship in cognitive & behavioural neurology at the UCLA Alzheimer disease research center. He is currently leading the neuropsychological unit in the department of clinical neuroscience, Geneva. His research work cover dementia, MCI and related disorders.

Karl-Olof Lovblad studied medicine at the University of Geneva, Switzerland. He was trained in Radiology and Neuroradiology at the university hospital in Bern. He also worked as a Research Fellow in MRI at the Beth Israel Deaconness Medical Center in Boston. In 2010, he was appointed Chairman and Professor of Neuroradiology at Geneva University Hospitals.

Habib Zaidi is Chief Physicist and head of the PET Instrumentation & Neuroimaging Laboratory at Geneva University Hospital and faculty member at the medical school of Geneva University. He is also a Professor of Medical Physics at the University Medical Center of Groningen (The Netherlands) and visiting Professor at Ecole Nationale Supérieure d'Electronique et de ses Applications (ENSEA, France). He received a PhD and habilitation (PD) in medical physics from Geneva University for dissertations on Monte Carlo modeling and quantitative analysis in positron emission tomography. Dr. Zaidi is actively involved in developing imaging solutions for cutting-edge interdisciplinary biomedical research and clinical diagnosis in addition to lecturing undergraduate and postgraduate courses on medical physics and medical imaging. He was guest editor for 5 special issues of peer-reviewed journals and serves as Editor-in-Chief for the *Open Medical Imaging Journal*, and Associate editor for leading journals in medical imaging. His academic accomplishments in the area of quantitative PET imaging have been well recognized by his peers and by the medical imaging community at large since he is a recipient of many awards and distinctions among which the prestigious *2003 Young Investigator Medical Imaging Science Award* given by the *IEEE*, the *2004 Mark Tetalman Memorial Award* given by the *Society of Nuclear Medicine*, the *2007 Young Scientist Prize in Biological Physics* given by the *International Union of Pure and Applied Physics* and the prestigious *2010 Kuwait Prize of Applied Sciences* (known as the *Middle Eastern Nobel Prize*) given by the *Kuwait Foundation for the Advancement of Sciences*. Dr. Zaidi has been an invited speaker of many keynote lectures at an International level, has authored over 330 publications, including ~140 peer-reviewed journal articles, conference proceedings and book chapters and is the editor of three textbooks on *Therapeutic Applications of Monte Carlo Calculations in Nuclear Medicine*, *Quantitative Analysis in Nuclear Medicine Imaging* and *Multimodality Molecular Imaging of Small Animals*. More details about this work can be found at http://pinlab.hcuge.ch/.